New insights into hydrothermal fluid circulation affected by regional groundwater flow in the Asal rift, Republic of Djibouti

Abdek Hassan Aden, Jasmin Raymond, Bernard Giroux, Bernard Sanjuan Sanjuan

energies

MDPI

Article

New insights into hydrothermal fluid circulation affected by regional groundwater flow in the Asal rift, Republic of Djibouti

Abdek Hassan Aden [1]*, Jasmin Raymond [1], Bernard Giroux [1] and Bernard Sanjuan [2]

[1] INRS-Institut National de la Recherche Scientifique, 490, Rue de la Couronne, Québec, QC G1K 9A9, Canada ; jasmin.raymond@inrs.ca
[2] BRGM, 3, Avenue Claude Guillemin, 45062 Orléans la CEDEX 02, France; b.sanjuan@brgm.fr
* Correspondence: Abdek.Hassan_Aden@ete.inrs.ca

Received: 20 January 2021; Accepted: 17 February 2021; Published: -----

Abstract: The Asal Rift hosts a lake located in a depression at 150 m below sea level, where recharge is influenced by regional groundwater flow interacting with the Ghoubbet Sea along the coast of Djibouti. This regional groundwater flow is believed to influence hydrothermal fluid circulation, which we aim to better understand in this study, having the objective of developing concepts for geothermal exploration in the area. To this end, magnetotelluric data acquired in the Asal Rift were processed and analyzed. 1D inversion models of electrical conductivity were interpolated for interpretation. These data were then used to build a 2D hydrogeological model, allowing multiphase flow and heat transfer simulations to be performed, considering the regional groundwater flow near the surface and the site topography, in order to confirm the preferred path of fluid flow. Geophysical data analysis indicates the presence of normal faults, notably the H fault, which may act as a conduit for the circulation of hydrothermal fluids and where the hanging wall can be a hydrogeological barrier within the hydrothermal system of the Asal Rift. The results from the 2D numerical flow and heat transfer modelling show the importance of groundwater flow responsible for thermal springs located at the periphery of Asal Lake. Reservoir temperature inferred by means of geothermometry ranging from 200 to 270 °C was shown to correspond to simulated temperature at potential reservoir depth. Moreover, simulated temperature between 600 and 1700 m depth is close to the temperature profile measured in the geothermal well Asal 6 of the area, with less than 20 °C difference. Simulations indicate that hydrothermal fluid circulation is likely influenced by the regional groundwater flow controlled by the topography and the major water bodies, the Ghoubbet Sea and Asal Lake, feeding buoyant fluids interacting with a deep magmatic source and where tectonic activity created normal faults offering a preferred path for fluid circulation.

Keywords: hydrothermal system; electrical conductivity; multiphase flow; numerical modeling; normal fault; heat source; Asal rift

1. Introduction

Extensive tectonic environments are known to host significant geothermal resources with large-scale fluid flows [1]. The Asal Rift is located in the central part of the Republic of Djibouti in the Afar depression, a tectonically active region where three major structures, the Great Rift Valley, the Red Sea, and the Gulf of Aden, are in extension and together form the Afar Triple [2,3], an emerged oceanic rift like that of Iceland. This region is a geological laboratory, where several scientific studies have been conducted to understand the processes and mechanisms related to the rifting phenomenon. The geological, geophysical, and geochemical studies carried out with French–Italian scientific collaboration between 1975 and 1988 guided the drilling of six deep geothermal exploration boreholes. A 3D geophysical model was built from passive seismic data [4] and indicated that the dip of normal faults far from the rift axis is about 50°–60° in the NE–SW direction, whereas normal faults

close to the rift axis are sub-vertical. The tectonic activity of these faults and the volcanism of the area, including the last eruption of the Ardoukoba volcano in 1978, are sources of seismic activity and drivers of hydrothermal fluid circulation. The results of seismic tomography indicate that most of the seismic events are located in the first 3 km below the surface [4]. Nevertheless, seismicity within the Asal Rift does not seem to be related to vertical fault planes, but rather to the opening of the fractures through a pressure gradient caused by hot fluids rising under the rift [5]. This mechanism implies that the planes of normal faults begin to tilt away from the rift axis [4] and could act as natural conduits allowing hydrothermal fluid circulation.

Asal Lake, which is 150 m below sea level, is affected by saline groundwater originating from the Ghoubbet sea located 12 km southeastward [2,3]. The role of normal faults in groundwater circulation in the Asal Rift appears important, especially for the circulation of groundwater interacting with Asal Lake, the Ghoubbet Sea, and the deep hydrothermal circulation of hot fluids, which has not been studied with modern physical models that can reproduce multiphase flow and heat transfer mechanisms. The present study is based on this hypothesis, for which work was conducted to better understand the importance of normal faults in the circulation of groundwater and hydrothermal fluids. This study was conducted in the context of geothermal exploration to provide fundamental knowledge analyzing the role of faults and considering the impact of groundwater flow between the Ghoubbet Sea and the Asal Lake. The work aims to define which faults can act as conduits or barriers to groundwater flow within the Asal Rift. To achieve this goal, electrical resistivity data were analyzed to build a conceptual model of the rift, followed by quantitative multiphase and heat transfer modelling of the hydrothermal system in 2D.

2. Geodynamic and hydrogeological context

The westward propagation of the Gulf of Aden at a velocity of 30 mm/year gave rise to the emergence of the Asal Rift [2]. The opening of the Asal Rift segment dates from the Miocene and its geology is characterized by the abundance of volcanic rocks formed in an environment of extension and opening. This emerged rift segment is 15 km long and 14 km wide. The opening velocity is approximately 16 mm/year [6] in the direction of N°45°E. The structure of this rift is characterized by a set of fracture networks and normal faults in the N130°E direction between Asal Lake and Ghoubbet Bay (Figure 1). Having a thin thickness and basaltic lavas at the surface in the form of basalt series, the land crust of the Asal Rift is considered transitional, i.e., an intermediate between the continental and nascent oceanic crust [4]. The first effusive event linked to the birth of the rift dates from 853,000 to 315,000 years ago [7]. Effusive magmatic activity continued in the northern part of the Asal Rift for 315,000 years and the southern part has been under seawater for 326,000 years, with the formation of hyaloclastites [7]. The activity of the central Fiɛale Caldera controlled the evolution of the rift between 326,000 and 100,000 years ago. Indeed, it allowed the injection of large volumes of basaltic lava into the interior floor that masked the previous faults [8]. Over the last 50,000 years, volcanic activity has decreased and the successive basaltic flow formations that make up Fiɛale Caldera have gradually been shifted by normal faults [7]. The modern rift structure began about 40,000 to 30,000 years ago with the development of the faults with outer margins H and δ [9]. From this period, the Fiɛale Caldera gradually extinguished and volcanic activity continued along the interior floor with small volcanic edifices and eruptive fissures [7]. With the most recent magmato-tectonic event dated in November 1978, two earthquakes of magnitude 5 and 5.3 were recorded in the Asal-Ghoubbet Rift and, following this event, 0.7 m of vertical subsidence and 2 m of horizontal extension in the direction N °40 E occurred in the rift [9]. A one-week eruption accompanied by basaltic fissures to the northwest of the rift gave rise in November 1978 to the axial volcanic chain and then to the eruption of the Ardoukoba volcano (Figure 1). At present, most of the rift deformation is concentrated in its northeastern part and around the edifice of the Fiɛale Caldera [4–6].

Thermal springs, fumaroles, and the existence of alteration on the surface of the Asal Rift are indicators of volcanic activity and the presence of potential geothermal resources at depth. Hot springs are abundant around the Asal Lake, especially in the eastern part, with temperatures ranging

from 30 to 90 °C (Figure 1). Between the Asal Lake and the Ghoubbet Sea, only fumaroles are observed at the surface because the hydrostatic level is below the topographic surface.

Chemical analyses of gases and determination of δD and $\delta^{18}O$ water stable isotopes of steam condensate have been performed for some of these fumaroles [10,11]. The results allowed estimating the source temperature at a depth higher than 230 °C, and even than 300 °C, in the studied Asal Rift. The isotopic data from the steam condensate suggest the existence of primary steam (likely separated at high temperature) originating from a deep heavy brine in this area [11]. The existence of this primary steam is in good agreement with the presence of a dominant vapor zone in the conceptual geothermal model proposed by BRGM [10–12].

Owing to the high salinity of Asal Lake and according to geochemical analyses, about 90% of the recharge of Asal Lake is believed to be due to infiltration and evaporation of Ghoubbet seawater [3], depleted in sulfate because of $CaSO_4$ precipitation [13]. From a geochemical study of water sampled from the rift thermal springs, the authors of [3] showed that the chemical and Sr isotope composition of these waters can be explained by variable seawater interaction with basaltic rocks at different temperatures and evaporation processes. Among thermal waters, those of the Manda group (Figure 1) indicate the lowest seawater–basalt interaction and evaporation degree, suggesting that their source temperature is not high and their circulation rate is relatively significant between the Ghoubbet Sea and the Asal Lake. The thermal waters of the Eadkorar group, located in the northeastern part of the lake (Figure 1), constituted by a mixing of seawater, Asal Lake water, and meteoric water, as suggested by the δD and $\delta^{18}O$ water stable isotopes [14,15], indicate the highest seawater–basalt interaction grade and seem to be the only direct leaks of a deep fluid discharged from a geothermal reservoir at 200–210 °C, as estimated by chemical geothermometry [3]. The Korilii and Kalou thermal waters (Figure 1) can result from a mixing between the deep geothermal water at 260–270 °C with seawater and Asal Lake water. The stable isotopes suggest the Korilii water is also diluted by meteoric waters [14,15]. The Eounda Alifitta waters, located in the north-eastern most part of the lake (Figure 1), indicate relatively low basalt–seawater interaction degrees and significant contributions of Asal Lake water. A contribution of meteoric water is also suggested by the water stable isotopes [15].

The geothermal wells A1, A3, and A6 are within a radius of 300 m (Figure 1). These wells have confirmed the existence of an intermediate reservoir located between 300 and 700 m depth, with a maximum temperature of 185 °C, and another potentially deep reservoir located between 1200 and 2000 m depth, with a maximum temperature of 260–280 °C (Figure 2). However, production tests proved to be ineffective for a continuous commercial geothermal energy production over time for two reasons:

- The geothermal fluid produced in the wells drilled south-west of the rift (wells A1, A2, A3, and A6), which reached the deep reservoir, had a salinity ranging up to 120 g/l, and wells were subject to scaling and corrosion problems. The solutions considered at that time with chemical inhibitors were not satisfactory [16].
- The wells drilled in the center of the rift (wells A4 and A5) intercepted formations with low permeability, even if a higher temperature (345 and 360 °C, respectively) was measured at their base.

The authors of [3] showed that the deepest geothermal fluid from the wells is constituted by a mixing of seawater and Asal Lake water, interacting with basalt rocks at 260–270 °C. The water stable isotopes also suggest a contribution of meteoric water [15], similar to that observed in the Korilii, Eadkorar, and Eounda Alifitta thermal waters, which could mainly be the meteoric water that transits from Asal local rift to Sakalol-Harralol depression, located at the north-west of Asal Lake, or/and the meteoric water coming from the deep circulating regional aquifers [11–14]. The low boron concentration observed in these deep waters suggests the existence of a steam phase in the geothermal system [3]. The existence of such a zone with dominant vapor is in agreement with the conclusions relative to the gas and steam condensate data drawn by [11] and the conceptual geothermal model proposed by BRGM [10–12]. The equilibrium temperature calculated from all gaseous reactive species associated with these well waters, except H2S, is very close to that measured at the bottom of the geothermal wells Asal 3 and Asal 6. This temperature corresponds to that of the

identified geothermal reservoir and varies between 250 and 270 °C. According to [3], the geothermal waters located at a depth between 300 and 700 m correspond to a mixing between the deepest geothermal fluid and seawater. The circulation of hydrothermal fluids in the northern part of the rift is believed to happen deeper than in its southern part [17].

Assuming the highly saline water of Asal Lake contributes to the recharge of the geothermal reservoir, this contribution is relatively recent as the water of Asal Lake was fresh and its salinity was recently acquired [3–9]. This constrains the fluid circulation time in the deep hydrothermal system located between 1 and 3 km, having high enthalpy. The water level of Asal Lake 9 to 6 thousand years ago was 160 m above sea level. Over the past 5 to 6 thousand years, the level has declined by 310 m and the lake level is currently 150 m below sea level [9]. This level has remained constant for the last centuries. Therefore, this suggests that, despite the intense evaporation from the arid climate of the area and the infiltration of water from the lake, this evaporation of lake water is compensated by a constant recharge mainly supplied by the Ghoubbet Sea.

The Asal 2 and Asal 3 wells are believed to penetrate the potential deep reservoir unit, but Asal 2 well was non-productive, although a temperature of 230 °C was measured at a depth of 923 m, while the Asal 3 and Asal 6 (located with a distance of about 300 m) were producers with permeable zones at a depth of 1030 m (Figure 2). The fluid produced was hyper saline and essentially composed of liquid at 260° C [16].

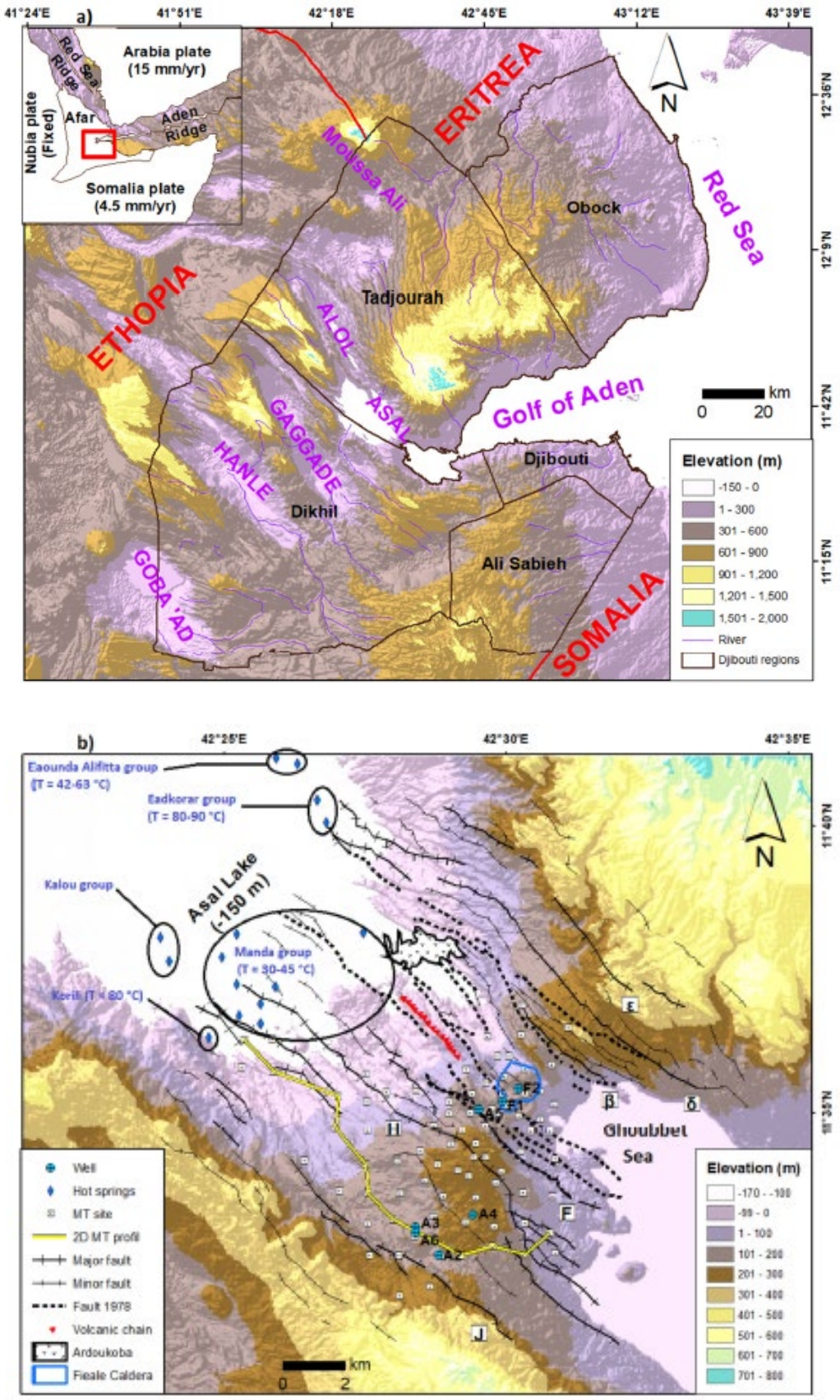

Figure 1. (a) Topography map of Djibouti with the main geothermal potential sites. Red rectangle is Djibouti. (b) Structural map of the Asal rift modified from [9]. EAR: East African Rift; MT: magnetotelluric.

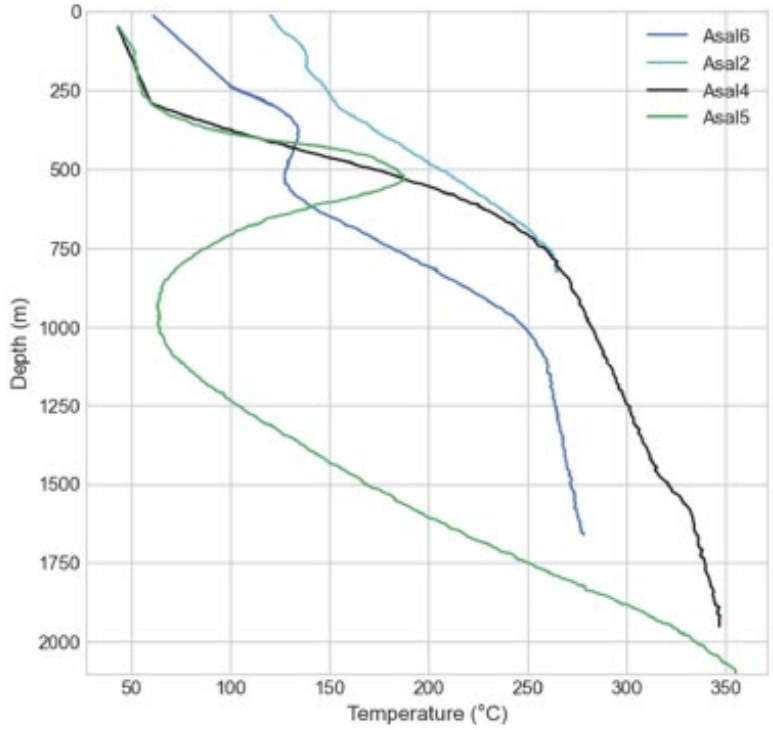

Figure 2. Temperatures measured at equilibrium in Asal geothermal wells.

3. Methods

An electrical resistivity model deduced from magnetotelluric surveys was used in this study to better understand the circulation of seawater through normal rift faults. Using the geoelectrical model, a 2D hydrogeological model was developed for numerically simulating multiphase flow and heat transfer, in order to better understand and quantify the flow dynamics and the development of possible hydrothermal reservoirs.

To better understand the role of seawater and the origin of thermal springs at the periphery of the Asal Lake, the 2D numerical model of coupled and multiphase flow and heat transfer was developed with the HYDROTHERM software provided by USGS [18,19].

3.1. Magnetotelluric data acquisition and processing

Generally, the presence of fluids in porous rocks and their interconnections, the types of minerals, and the temperature and pressure in the rocks contribute to the variation of electrical resistivity. Hydrothermal fluids and the existence of a layer of clay that acts as a cap rock present on the roof of a hydrothermal reservoir are usually identified as highly conductive areas, while, on the other hand, gas reservoirs and cooled magma are identified as less conductive areas [20].

Between 2007 and 2008, a survey including 81 magnetotelluric (MT) stations was carried out in the Asal Rift by the Icelandic company ISOR [16]. The geographical distribution of the MT stations, which are roughly 1 km apart, covers a large part of the Asal Rift Figure 1). The instrument used to record the data was a Phoenix MTU-5 system and has the ability to record the temporal variation of the three components of the magnetic field (Hx, Hy, and Hz) and the two components of the telluric field (Ex and Ey). A reference station, located 10 km from the study area, was used to correct and reduce the local noise of the MT signals [21]. The data collection time was 48 h. For each site, time series were converted from time domain to frequency domain impedance tensor [22]. The frequency range of the data varies from 12.9*10-6 Hz to 400 Hz and corresponds approximately to a depth of investigation of the MT signal of more than 12 km inside the earth.

In this study, a 1D inversion of each station of the MT data was achieved. The apparent resistivity of the squared sum of the components of the invariant impedance [23] was inverted using the Occam algorithm [24]. This impedance is expressed as follows:

$$Z_{ssq} = \sqrt{\frac{Z_{xx}^2 + Z_{xy}^2 + Z_{yx}^2 + Z_{yy}^2}{2}} \quad (1)$$

where Zxx, Zxy, Zyx, and Zyy are the elements of the impedance tensor Z. Generally, the invariant determinant model is used, but, recently, [25,26] have shown that the determinant model is affected by galvanic distortion at depth. These authors argue that this model tends to reveal more conductive geological structures in the presence of distortion. Another invariant type of model named SSQ (sum of squared elements) is used because it is less affected by the distortion and more appropriate to obtain a first representative approximation of the regional electrical resistivity [25,26].

In this study, an uncertainty of 10% apparent resistivity was assigned for several soundings, except seven soundings with up to 20% uncertainty. The signal in the so-called dead-band, which corresponds to the 5 to 20 s period interval, was low and the resulting uncertainty higher. Moreover, the uncertainty assigned for the phase was 2.5°. With this approach, an electrical resistivity model was developed, where data from all sites were interpolated and interpreted to infer concepts about underground fluid flow. The inversion results of an electrical conductivity model are presented in Section 4 below, helping to evaluate the role of the Asal Rift in groundwater circulation interacting with deep hydrothermal fluids and to delineate the presence of a hydrothermal system located at a depth between 1.2 and 2 km.

3.2. Conceptual model and numerical simulations

High enthalpy geothermal resources required to generate electricity are generally found in areas where magma is introduced into the shallow crust (<10 km) and hydrothermal convection takes place over intrusive hot bodies. For a convective-type geothermal system such as the Asal Rift, the most appropriate conceptual model consists of the following elements [27]. A deep magmatic intrusion that is covered by a host rock. The latter hosts permeable reservoir formations that are covered by a cap rock close to the surface. Based on the structure of this type of geothermal system and the results of the geothermal wells data (Figure 2), a conceptual model of the Asal Rift was set up, helping to approximate the thickness of the seawater intrusion towards Asal Lake. The 2D conceptual model used to define the geometry of the numerical model was based on an interpreted resistivity section inferred from the 1D electrical resistivity model developed in this study. This 2D section is parallel to the rift axis (Figure 1) and was chosen because of the presence of productive geothermal wells (Asal 3 and Asal 6) along this section, and is parallel to the believed direction of regional groundwater flow. The temperature profile of the Asal 6 well was used to calibrate the numerical model.

3.2.1. Multiphase flow and heat transport

Simulation of multiphasic flow and heat transport is challenging because it is difficult to consider the critical point to set the appropriate thermodynamic state of the fluid in two phases. The pressure–enthalpy formulation that defines the thermodynamic state of the fluid in two phases can be used to avoid this problem, which was done in the HYDROTHERM code [28]. The governing equations used in the HYDROTHERM code are expressions of mass and energy conservation formulated in terms of pressure and enthalpy. As no potentiometric-head function exists for density fields that depend on temperature, pressure is chosen as the dependent variable for fluid flow. All pressures are expressed as absolute and the water-component flow equation is based on the conservation of water mass in a volume element, coupled with Darcy's law for multiphase flow through a porous medium [19]:

$$\frac{\partial}{\partial t}[\varphi(\rho_w S_w + \rho_s S_s)] - \nabla.\frac{k k_{rw}\rho_{rw}}{\mu_w}[\nabla P + \rho_w g] - \nabla.\frac{k k_{rs}\rho_{rs}}{\mu_s}[\nabla P_g + \rho_s g] - q_{sf} = 0 \quad (2)$$

where φ is the porosity (dimensionless), ρ is the fluid density (kg m^{-3}), S_w is the saturation of liquid phase (water) and S_w is the saturation of the gas phase (steam or air; dimensionless), k is the porous-medium permeability tensor (m^2), k_r is the relative permeability (dimensionless), μ is the viscosity of fluid (Pa s), P is the fluid pressure in the liquid phase (Pa), P_g is the fluid pressure in the gas phase (Pa), g is the gravitational constant (m s^{-2}), q_{sf} is the flow-rate intensity of a fluid-mass source (positive is into the region) (kg s^{-1} m^{-3}), t is the time (s), and ∇ is the spatial gradient (m^{-1}). The phase subscripts w and s refer to water (liquid phase) and steam (gas phase or vapor phase), respectively. In the single-component (water) zone, $p_g = p$ because the capillary pressure is assumed to be zero. As any point in the mesh, it can be a single component or two component zone and the saturation constraint is $S_w + S_g = 1$.

The thermal-transport equation is based on the conservation of enthalpy in both the fluid phases and the solid phase of the porous medium, in a volume element of the region. So, enthalpy is a derived property containing both internal energy and flow energy. Thus,

$$\frac{\partial}{\partial t}[\varphi(\rho_w h_w S_w + \rho_s h_s S_s) + (1 - \varphi\rho_r h_r] - \nabla . K_a I \nabla T + \nabla . \varphi(\rho_w h_w S_w v_w + \rho_s h_s S_s v_s) - q_{sh} = 0 \quad (3)$$

where h is the specific enthalpy of the fluid phase (J kg^{-1}), h_r is the specific enthalpy of the porous-matrix solid phase (J kg^{-1}), ρ_r is the density of the porous-matrix solid phase (kg m^{-3}), K_a is the effective thermal conductivity of the bulk porous medium (combined liquid, gas, and solid phases) (W m^{-1} °C^{-1}), I is the identity matrix of rank 3 (dimensionless), T is the temperature (°C), q_{sh} is the flow-rate intensity of an enthalpy source (positive is into the region) (W m^{-3}). The phase subscripts w and s refer to water and steam respectively.

The main assumptions underlying Equations (2) and (3) that are solved in HYDROTHERM are the following: capillary pressure effect is negligible, porous medium and fluid are in local thermal equilibrium, the fluid is pure water, heat transfer by radiation and dispersion can be neglected, Darcy's law is valid with two phase forms, and relative permeability is a nonhysteretic function of liquid volume saturation.

3.2.2. Spatial and temporal discretization

The 2D conceptual model to simulate extends 14 km horizontally (Figure 1) and 3 km vertically from the land surface. The model geometry in the HYDROTHERM simulator is discretized with a regular 100 × 100 grid. The simulation time span to reach a quasi-steady state temperature regime was 100,000 years and an initial time step of 0.001 year was considered. An automatic time step algorithm is used in the simulator, where smaller time steps are selected when conditions are changing rapidly and maximum values for changes in pressure, enthalpy, and liquid saturation are specified before running the simulation [19]. In our study the maximum changes in pressure, enthalpy, and saturation are 10%, 5%, and 0.03, respectively. This results in a maximum time step of 1000 years. The independence of the mesh is presented to demonstrate the accuracy of the solution. In this study, two different grids were considered with two different initial time steps.

3.2.3. Initial and boundaries conditions

Numerical modeling of continental or subaerial hydrothermal systems often considers the upper system flow boundary to be the water table of shallow aquifers affected by topography [18,29,30]. Therefore, initial conditions are an initial temperature of 20 °C with an atmospheric pressure of 1 atm at the surface of the 2D model, a geothermal gradient of 49 °C/km, and hydrostatic pressure increasing with depth. A heat flux of 100 mW/m^2 was fixed at the base of the model and the surface boundary has a constant temperature of 20 °C. A pressure of 1 atm was also considered at the surface boundary. The base of the model is considered impermeable with no flux. Constant temperature and pressure determined from the initial conditions were imposed on the lateral boundaries of the model in order to take into account the variation of the geothermal and the pressure gradients at depth. This allowed to establish the temperature and pressure gradients according to the topography and the

water table depth inferred from the conceptual model. Five different simulation scenarios are presented below. For all scenarios, a deep resistive structure named R2 was taken as a magmatic intrusion or heat source, and a heat flux of 2700 mW/m^2 was fixed at the base of this R2 structure. This is the base case scenario where the boundary conditions presented above are used.

Numerical simulations conducted in magmatic hydrothermal systems [18,31] showed that the representation of the topography is an important factor to reproduce regional groundwater flow driven by the topography. This was taken into account to better evaluate the dynamic of groundwater flow between the Asal Lake and Ghoubbet Sea. In addition, the influence of infiltration from rainfall in geothermal systems is not negligible, but the impact of rainfall in the hydrothermal activity is commonly limited in the upper part [32] and may not prevail in the deeper part of the hydrothermal system, as in the case of Asal Rift. The impact of rainfall was not simulated as the numerical simulations considered confined flow.

3.2.4. Hydraulic and thermal properties

The geological units considered in the conceptual 2D model were interpreted from the 1D electrical resistivity model developed in this study. Hydraulic and thermal properties of each unit were defined according to Table 1, used as the base case scenario and noted as scenario 1. Then, four other different scenarios were conducted in order to evaluate the sensitivity of the results to changes in the main hydraulic parameter (permeability) of the geological units. Three permeable vertical conduits that can be associated with fault zones were added and coexist to evaluate the possible impact of fault zones. The choice of emplacement and geometry of these faults was based on the interpretation of the inverted electrical resistivity profile developed in this study. Thus, properties of faults remain the same of those of unit C1 (Table 1), but with higher isotropic permeability equal to 2.17×10^{-14} m^2. In scenario 2, a permeability dependent temperature in the potential deep reservoir unit was adopted with an isotropic permeability of heat source equal to 10^{-17} m^2. Scenario 3 was simulated to understand the behaviour of the system in the deeper part without permeability dependent temperature. To do this, an isotropic permeability was assigned to both the heat source (10^{-17} m^2) and the potential deep reservoir unit (10^{-15} m^2). This permeability value assigned in the potential deep reservoir unit is of the same order of the one estimated from the production test of well Asal 3, which reached the potential deep reservoir, which was equal to 6.3×10^{-15} m^2 [33]. The conditions of scenario 4 are similar, but a permeability dependent temperature inside the heat source unit was used. Finally, scenario 5 was simulated with permeability anisotropy within the near-surface aquifer C1, which was assigned to the model to investigate how it can influence the regional groundwater flow. Horizontal permeability was set one order higher than the one of the base case scenario. The purpose of this scenario 5 was to simulate the predominance of horizontal fluid movements over vertical movements within this geological formation and hypothesize the behaviour of the system in such conditions. The properties of all units remain the same as those of scenario 1, except for the horizontal permeability in the unit C1, which was equal to 2.17×10^{-14} m^2.

In the crust, thermal conductivity decreases with increasing temperature [34]. The formulation developed by [34] for crystalline rocks with a temperature range between 20 and 500 °C was taken into account, where the thermal conductivity value at 20 °C is 2.5 W m^{-1} °C^{-1}. To consider the effect of latent heat of crystallization, a linear temperature-dependent rock heat capacity relation was adopted, which doubles from 900 at temperatures below 100 °C to 1800 J kg^{-1} at temperatures greater than 500 °C. This linear relationship was based This linear relationship was based on the approach initially developed by [34] and then used by [35] for similar modeling work.

Temperature-dependent rock permeability was formulated for both the potential deep reservoir and heat source (Table 1). This formulation is the same as that developed by [29] for magmatic hydrothermal systems, where permeability increases with the decreasing temperature. Thus, the permeability of the heat source with a temperature range of 400–500 °C is one order of magnitude less than the one of the deep reservoir with a temperature range of 200–400 °C.

In such systems, fluid flow is mainly controlled by processes such as thermal pressurization, buoyancy, and magmatic exsolved fluid. Our hypothesis is based upon the existence of deep

hydrothermal circulation in the Asal Rift and the absence of a magma chamber at a depth less than 5 km [4]. Thus, the fluid pressure originating from the heat source unit may have allowed rocks to fail and created permeability within the potential deep reservoir unit.

Table 1. Hydraulic and thermal properties for simulation of the base case scenario.

Formations unit	**Unsaturated formation: R1**	**Aquifer: C1**	**Cap rock: C2**	**Potential deep reservoir**	**Heat source : R2**
Porosity (-)	0.12	0.12	0.12	0.27	0.12
Horizontal permeability (m^2)	2.17×10^{-16}	2.17×10^{-15}	2.17×10^{-18}	Temperature dependent	Temperature dependent
Vertical permeability (m^2)	2.17×10^{-16}	2.17×10^{-16}	2.17×10^{-18}	Temperature dependent	Temperature dependent
Thermal Conductivity ($W\ m^{-1}\ k^{-1}$)	Temperature dependent	Temperature dependent	Temperature dependent	Temperature dependent	Temperature dependent
Density ($kg\ m^{-3}$)	2700	2700	2700	2800	2900
Specific heat ($J\ kg^{-1}$)	1000	1000	1000	Temperature dependent	Temperature dependent
Compressibility (Pa^{-1})	10^{-20}	10^{-20}	10^{-20}	10^{-20}	10^{-20}

4. Results

The results of 1D electrical conductivity model are initially presented and followed by the results of fluid flow simulations.

4.1. 1D electrical resistivity model

Observed and simulated electrical resistivity fits with an average root mean square (RMS) misfit of about 0.1. The match of electrical resistivity and phase at each MT station appears reasonable, as can be seen for resistivity, and phase curves of all MT sites along the 2D MT profile (Figure 1) are presented in Figure 3.

The H fault (Figure 1, Figure 4) delineates two distinct zones of electrical resistivity. The north-east part of this fault is defined as a conductive zone, while the south part is less conductive (more than 20 Ω.m). The geometry of the Fiεale Caldera corresponds to a well-defined zone of electrical resistivity of the order 20–30 Ω.m (Figure 1, Figure 4). The different electrical iso-resistivity maps in Figure 4 show a gradient of electrical conductivity that increases in the direction from the south-west to the north-east. This change of the conductivity gradient is clearly visible and evident at depths of 1640 and 1840 m (Figure 4).

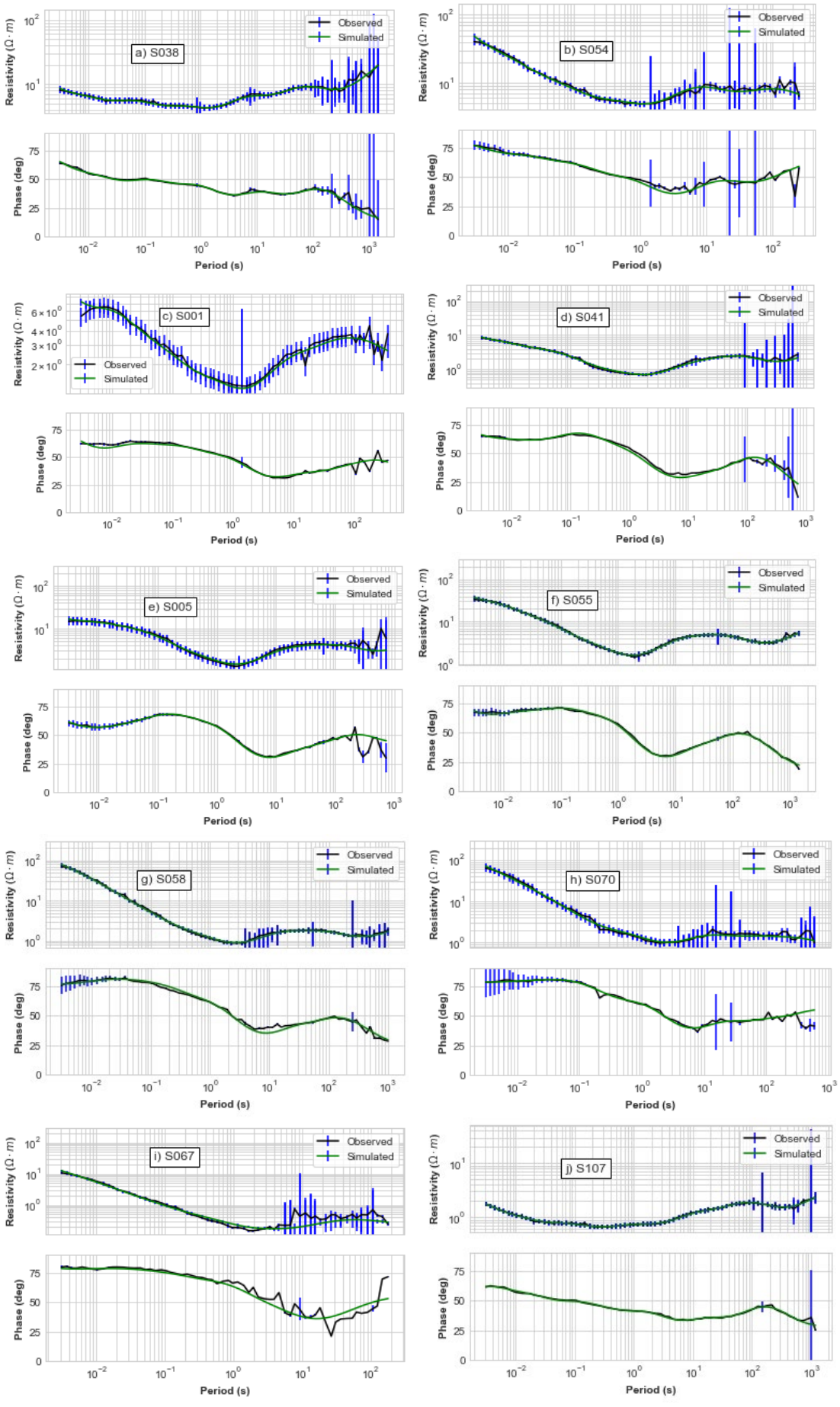
a) S038
b) S054
c) S001
d) S041
e) S005
f) S055
g) S058
h) S070
i) S067
j) S107
Observed
Simulated
Resistivity (Ω · m)
Phase (deg)
Period (s)

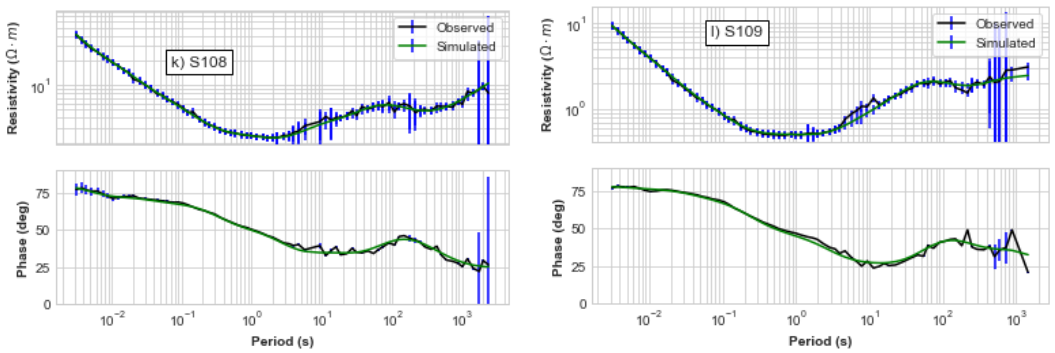

Figure 3. Comparison of observed and simulated electrical resistivity at MT sites along 2D MT profile in Figure 1.

4.2. 2D conceptual model

The conceptual model of Figure 5 was defined using the available electrical resistivity data interpreted along a cross section more or less parallel to the Asal rift axis (Figure 1). A top layer of high resistivity (R1) is associated with unsaturated formation near the surface. The underlying layer with a low resistivity C1 is considered as an aquifer, which can host shallow or intermediate reservoirs, as evidenced by temperature profiles of wells Asal 6 and Asal 3 (Figure 2). These temperature profiles show convection cells with a change in geothermal gradient at a depth between 300 and 600 m that can only occur in permeable layers with fractures.

Layer C2 can be a cap rock covering the formations hosting deep hydrothermal reservoirs, which is referred to here as the potential deep reservoir unit in the numerical model. The highly resistive R2 structures can mostly likely be associated with intrusive bodies.

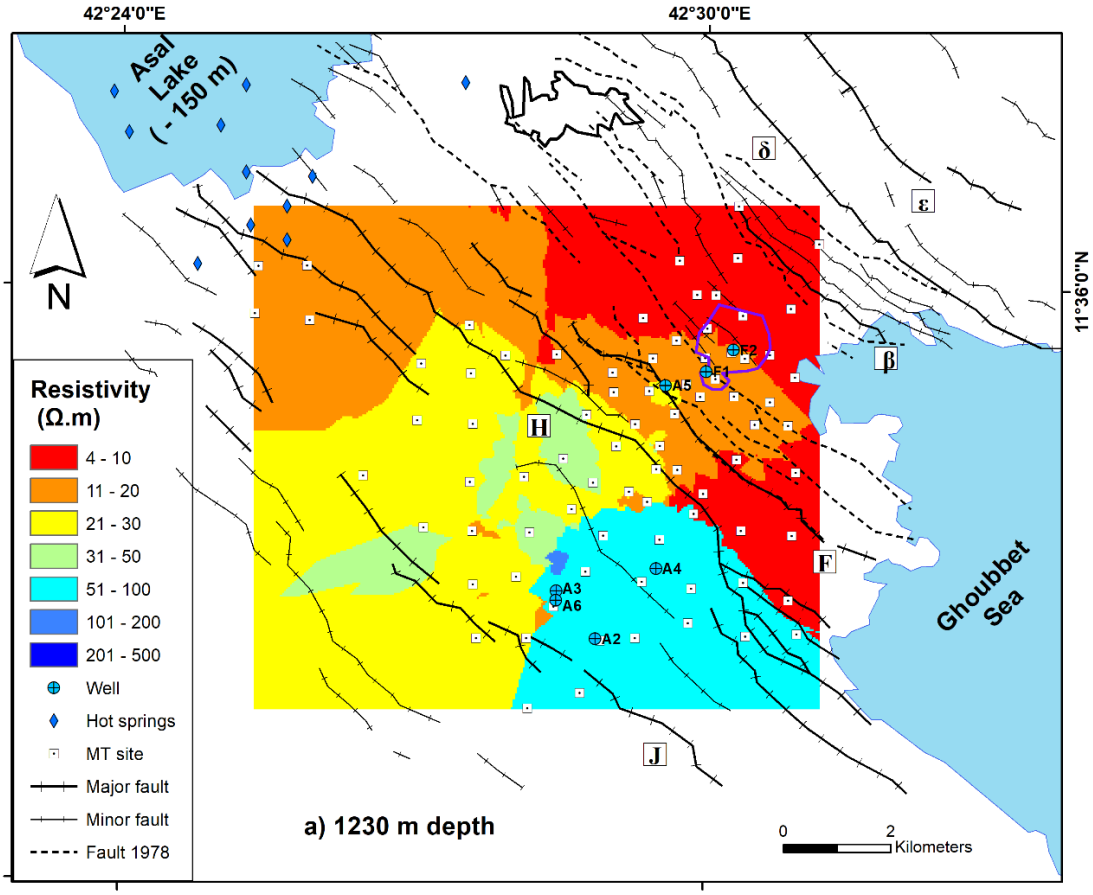
42°24'0"E
42°30'0"E
11°36'0"N
Asal Lake (- 150 m)
N
Resistivity (Ω.m)
4 - 10
11 - 20
21 - 30
31 - 50
51 - 100
101 - 200
201 - 500
Well
Hot springs
MT site
Major fault
Minor fault
Fault 1978
δ
ε
β
H
F
J
F1
F2
A2
A3
A4
A5
A6
Ghoubbet Sea
a) 1230 m depth
0
2
Kilometers

433

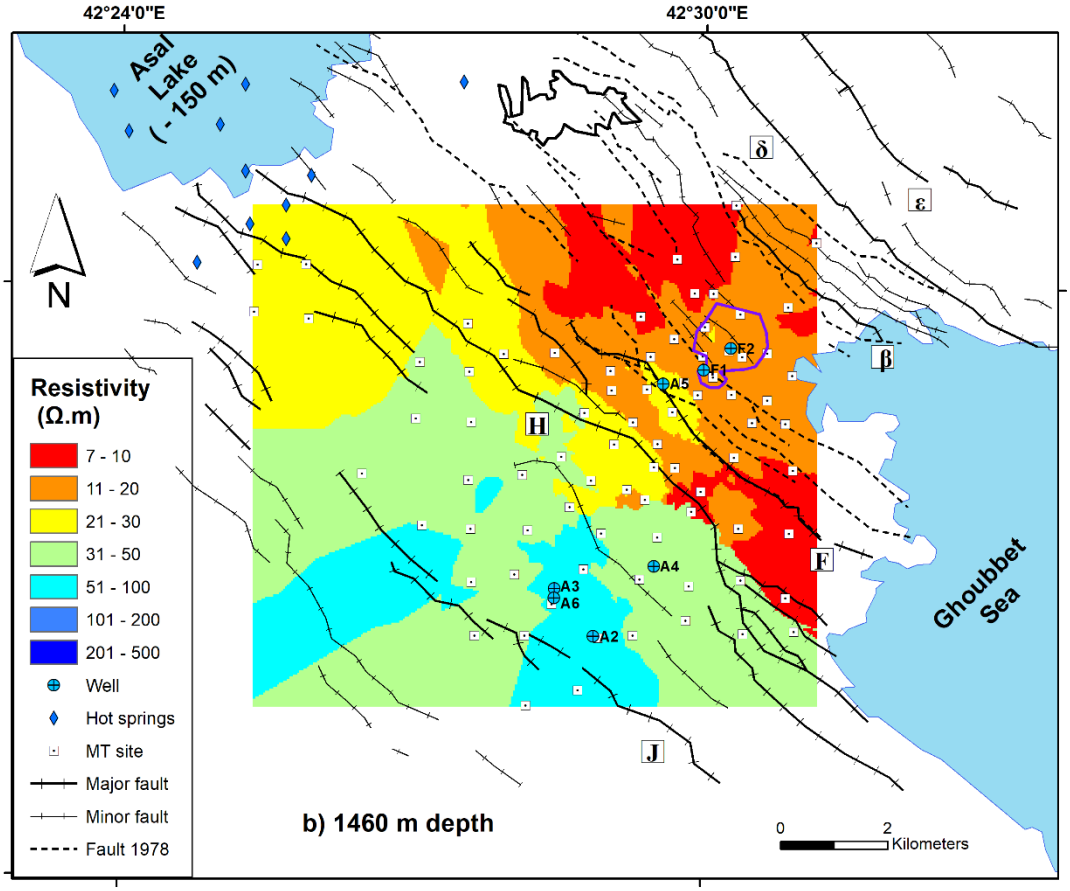
42°24'0"E
42°30'0"E
11°36'0"N
Asal Lake (- 150 m)
N
Resistivity (Ω.m)
7 - 10
11 - 20
21 - 30
31 - 50
51 - 100
101 - 200
201 - 500
Well
Hot springs
MT site
Major fault
Minor fault
Fault 1978
δ
ε
β
H
F
J
F1
F2
A2
A3
A4
A5
A6
Ghoubbet Sea
b) 1460 m depth
0
2
Kilometers

434

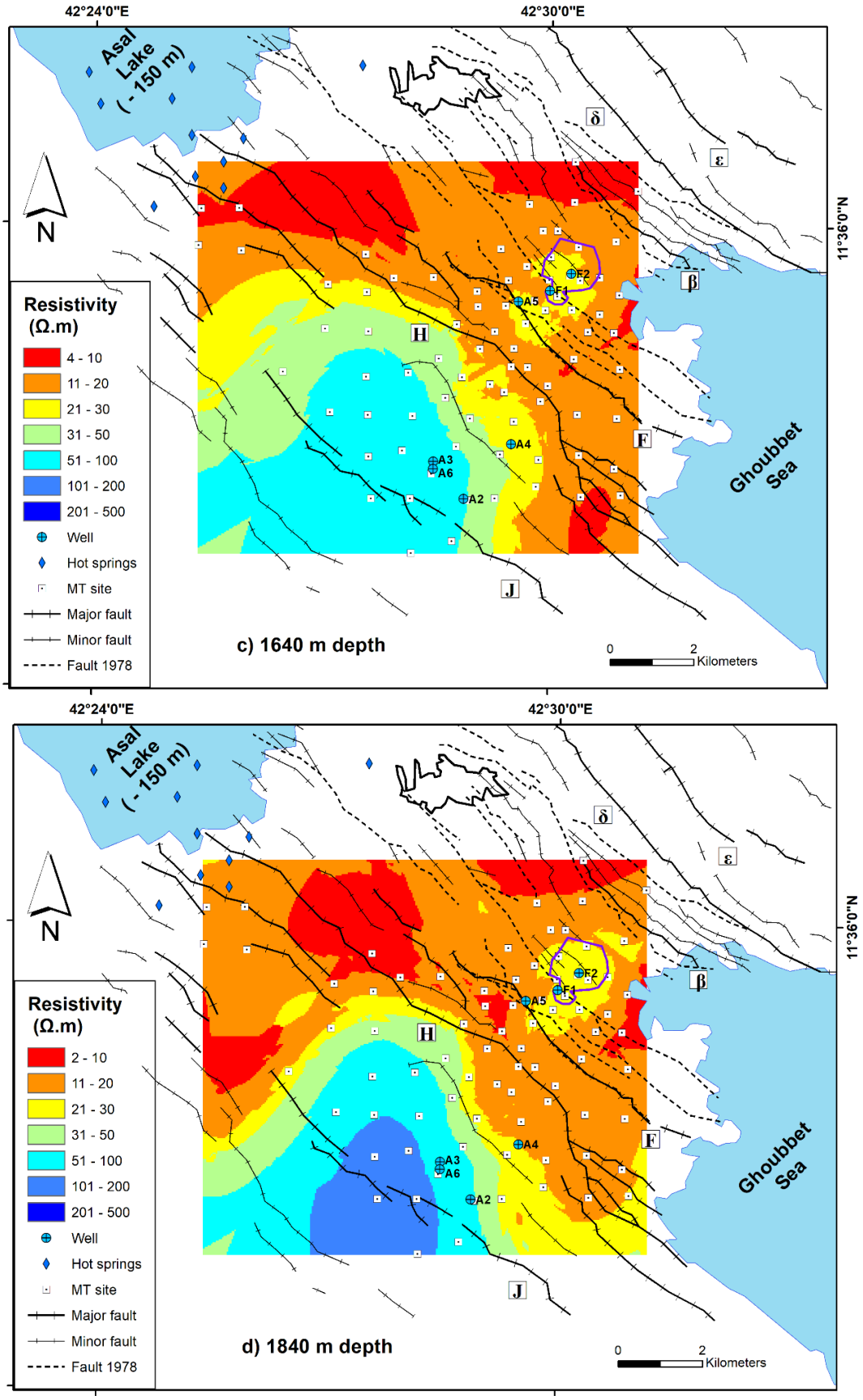

Figure 4. Interpolation at selected depth of inverted electrical resistivity.

.

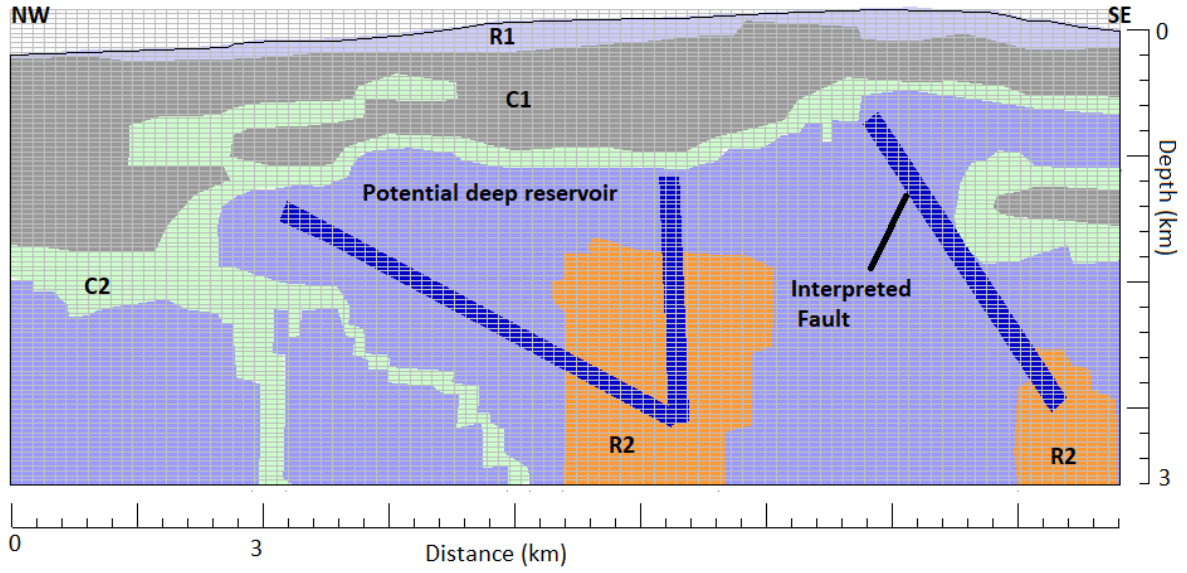

Figure 5. 2D conceptual model interpreted from along 2D MT profile in Figure 1.

4.3. Numerical simulations

Mesh and time step independence were investigated to make sure numerical simulations are reliable. A comparison between different grids for scenario 1 at the location of Asal 6 well at a depth of 1500 m is presented in Appendix A. The results with a 100 × 100 grid and initial time step of 0.001 year are presented in Figure 6 and 7. Furthermore, a mesh with a 40 × 100 grid with an initial time step of 0.01 year was considered (Figure 6) and the patterns of flow and heat transport observed were similar to those of mesh with a 100 × 100 grid (Figure 7). We can deduce and argue that our solution is independent of the choice of the grid and the choice of the initial time step. One should keep in mind that the HYDROTHERM software uses an algorithm allowing an automatic time step [19] in which only the initial time step is set by the user.

The simulation results of scenario 1 and scenario 2 (Figure 6 and 7) show the upwelling of a warm fluid or an upflow zone that propagates from the heat source at the model center toward Asal Lake and toward the sea, but to a lesser intensity. The development of convection movements is visible inside the deep potential reservoir unit that can likely host localized hydrothermal reservoirs. Scenarios 3 and 4 present similar flow and temperature patterns with the presence of three flow zones at a distinct depth. Groundwater circulation toward Asal Lake inside the aquifer C1 can be identified and the widening of the deep upflow zone of hydrothermal reservoir from the center to the sea can be observed. High velocity flow vectors also appear in the center of the rift at a depth between 900 and 1800 m, particularly inside the faults zones, where hot ascent fluid in the fault close to the sea and cold descendant fluid in the fault close to Asal Lake can be observed. This can be associated with a mixture of descending cold groundwater with the ascending deep hydrothermal circulation over a depth of about 500 m and driven by the temperature gradient (Figure 7). Scenario 5 captures the same temperature patterns as the results of scenarios 1 and 2, but with strong flow vectors inside the unit called C1, noted here as a shallow aquifer. Obviously, the system behaviour remains the same in the deeper part even with the presence of significant lateral flow in the upper part of the system (Figure 7).

The Asal 3 and Asal 6 wells are believed to be penetrating the deep potential reservoir unit. The full comparison between simulated and observed temperature in well Asal 6 for each scenario is shown in Figure 8. The simulated temperature is about 255 °C in scenario 1 at a depth of 1600 m, which approximately corresponds to the measured temperature at the bottom of Asal 6 well (265 °C at a depth of 1700 m). In fact, the measured temperature matches with the simulated temperature of scenarios 1, 2, and 5, except in the upper part above 600 m depth (Figure 8). The comparison between

the measured and simulated temperature for scenario 3 is not presented as it is the same as scenario 4 (Figure 8).

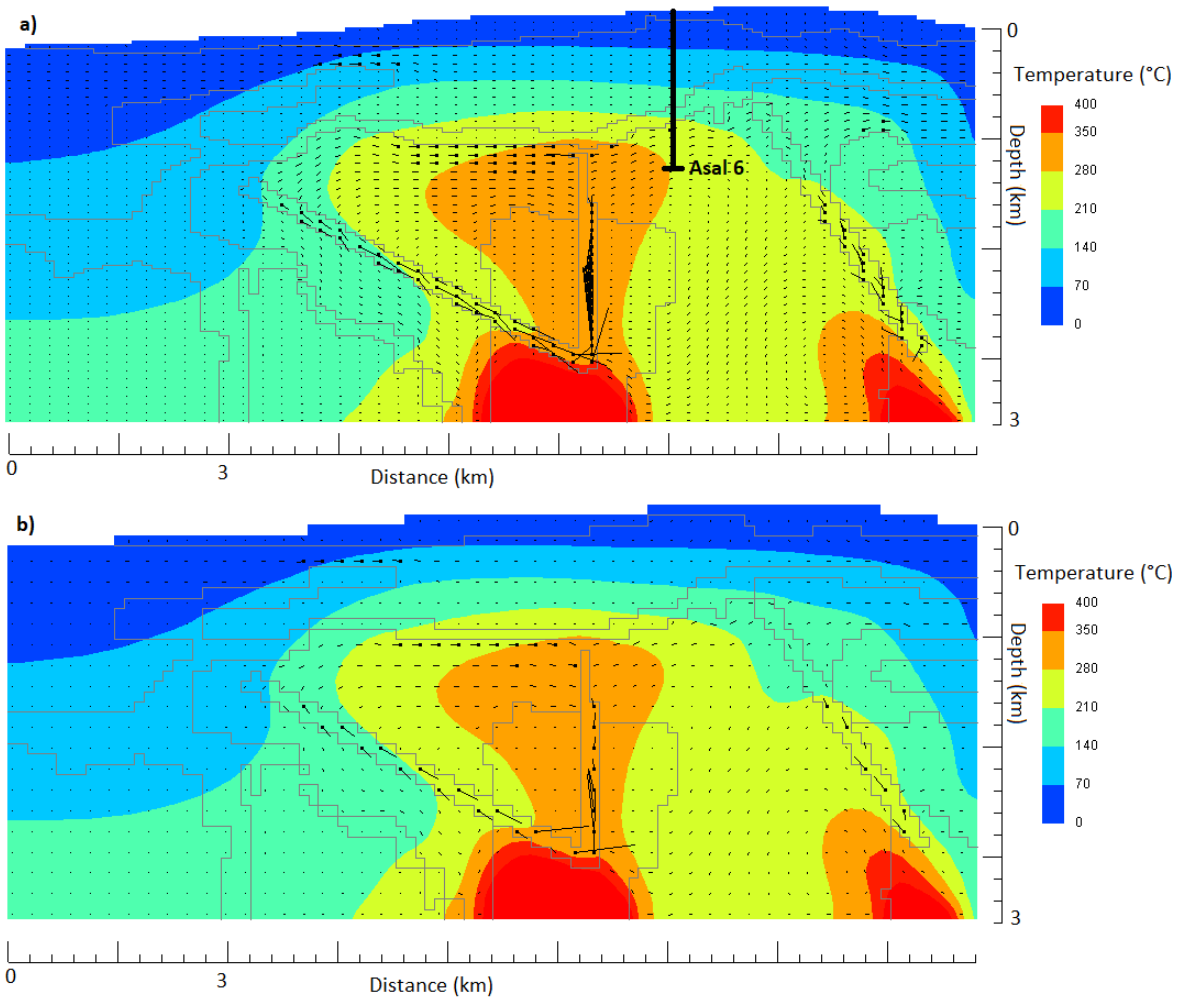

Figure 6. Simulated temperature and flow vectors at time equals to 100,000 years in scenario 1. The direction of flow is from the point to the end of the straight lines. The length of each line indicates the water flow vector magnitude, where 1.2 km = 1 x 10^{-5} g (s^{-1} cm^{-2}). (a) Results with a grid of 100 x 100 and initial time step of 0.001 year. (b) Results with a grid of 40 x 100 and initial time step of 0.01 year.

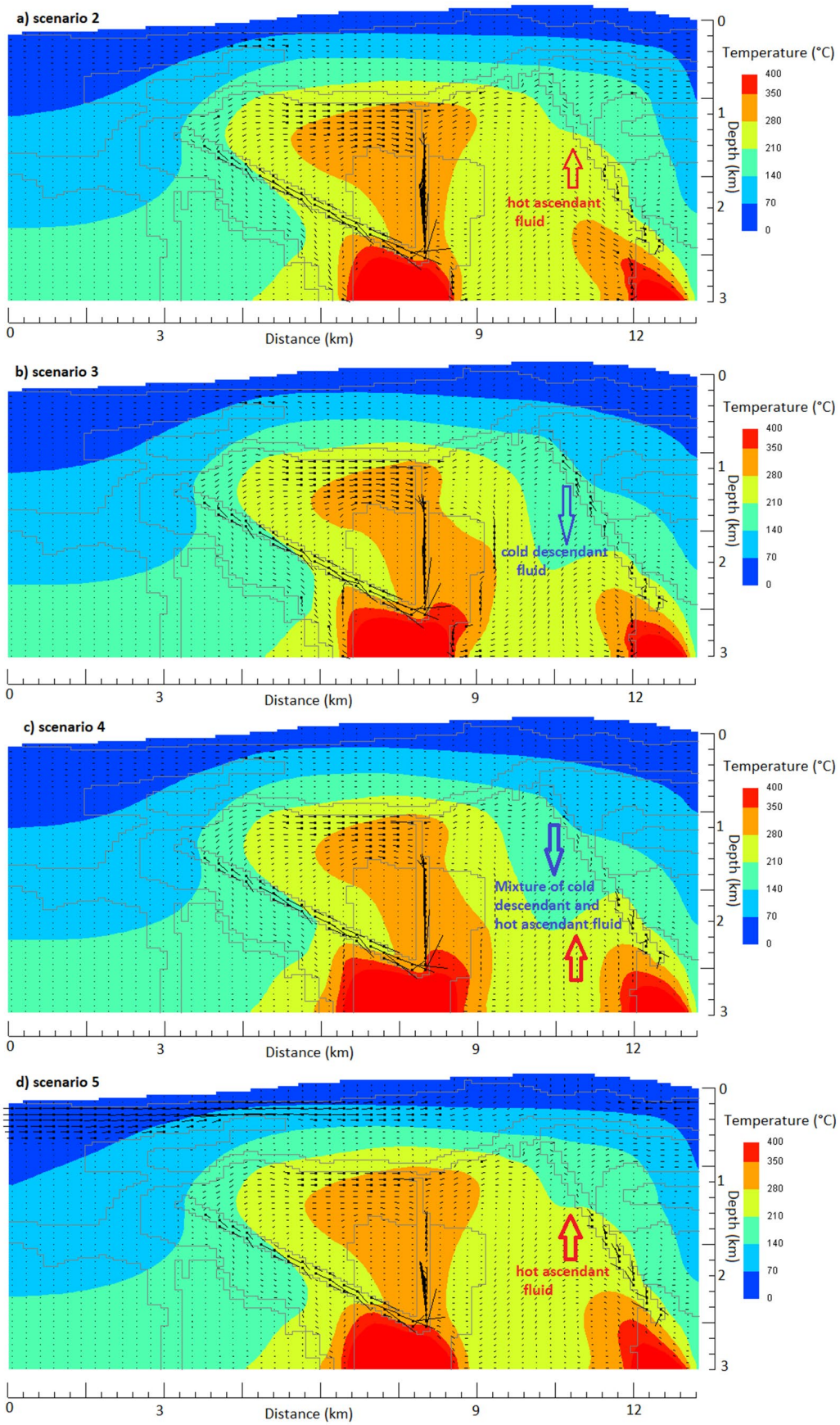

Figure 7. Simulated temperature and flow vectors at time equals to 100,000 years. The direction of flow is from the point to the end of the straight lines. The length of each line indicates the water vector magnitude, where 1.2 km = 1 x 10^{-5} g (s^{-1} cm^{-2}).

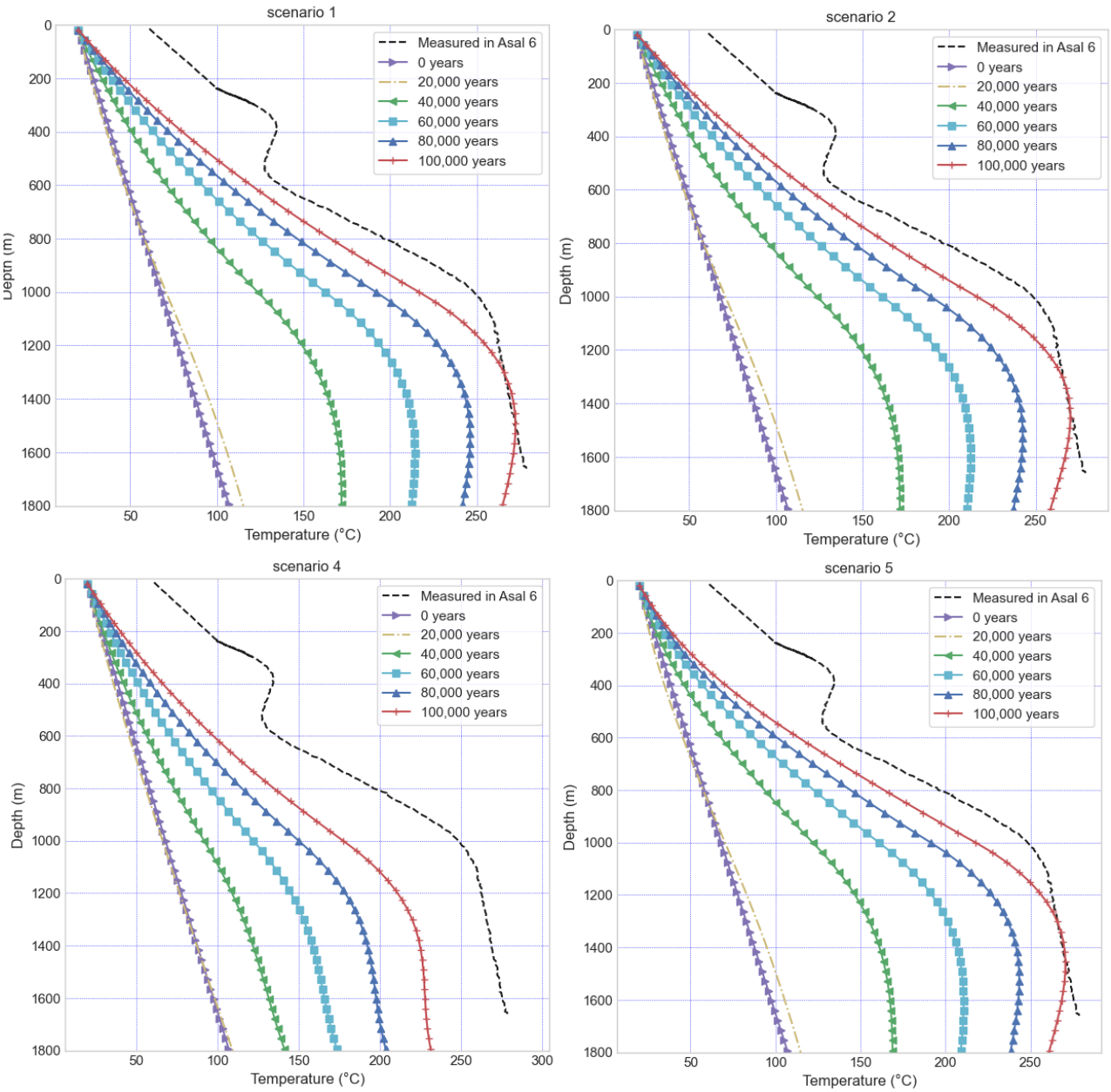

Figure 8. Comparison between the observed and simulated temperatures at well Asal 6.

5. Discussion

The directions of faults and fractures are parallel to the direction of believed groundwater flow (Figure 1 and 4). Unfortunately, the available MT data do not cover the entire area of the emerged Asal Rift. A lack of data in the area of the normal faults ε and δ to the north-east of the rift limits the interpretation (Figure 1). However, previous geochemical analyses conducted by [36] in littoral thermal springs could help to place our interpretations in a logical context and may explain the origin and the evolution of thermal waters that are not far at the eastern flank of the normal faults ε and δ located at the north-east of the rift. These authors conclude that a mixture of hot seawater with cold seawater emerges through the fractures. Moreover, the presence of deep hot seawater-derived geothermal fluid with a temperature of 210 °C was confirmed [37]. Despite the lack of data in this zone, our interpretation of pronounced fluid circulation at the north-east of the rift can be justifiable. The comparison between the 87Sr/86Sr ratio and strontium concentration of the brine waters from

512 the Red Sea bottom and Asal Lake have indicated that Asal Lake is a better location to study how
513 hydrothermal fluids of seawater origin may evolve in the Red Sea rift [38].
514 The descriptive lithology of the wells drilled in the Asal Rift consists mainly of a succession of
515 basaltic series, which were deposited over geological time and have different ages [39]. Even if the
516 abundance of shale and/or graphite is known to cause a decrease in electrical resistivity [21], no
517 significant quantity of the latter is found in the wells drilled, and more precisely between 1 and 2 km
518 depth [39]. Within the Earth's crust, the dominant electrical conduction mechanism is electrolytic [21].
519 Therefore, low electrical resistivity in the context of the Asal Rift is generally interpreted as an
520 indicator of the presence of a fluid. At depths of 1200 and 1400 m (Figure 4), groundwater seems to
521 be present mainly between the H fault and the δ fault according to the following evidence. In this
522 zone, observed fractures were caused by the tectonic and volcanic activity associated with the
523 eruption of the Ardoukoba volcano that occurred in 1978 (Figure 1). The low electrical resistivity
524 suggests the presence of water and hence more important flow to the southeast between the H and F
525 faults, and to the north-east of Fiɛale Caldera. The existence of dykes at a depth near the rift axis
526 (between the F and β faults) has been hypothesized based on the deformations observed at the surface
527 [9]. In this case, rift extension and subsidence are controlled by dyke injection. Moreover, the
528 stretching model of Asal Rift is likely accommodated by the magma activity [40]. This extension can
529 result in open cracks where groundwater flows easily. The proximity of the sea and the coexistence
530 of recent open faults and fractures is a fair evidence for such flow illustrated with the simulations.
531 The electrical resistivity model, especially images obtained at a depth between 1.2 and 2 km
532 (Figure 4), indicates a possible hydrothermal system in the north-east part of the Asal Rift and with
533 more pronounced regional groundwater flow in this area rather than in the south-west zone
534 (Figure 4). Considering the contrast in electrical resistivity between the north-east and south-west
535 parts of the Asal Rift, it seems likely that the hanging wall of the H fault acts as a hydrogeological
536 barrier separating the Asal Rift between two zones. A first conductive zone, whose high electrical
537 conductivity is due to the presence of groundwater, as well as a second less conductive zone with an
538 increase of the electrical resistivity gradient towards the south of the rift, imply lower porosity and/or
539 less groundwater in pore space and fractures. Only the major J fault and the minor fault passing
540 through well Asal 4 exist in the south zone of the Asal Rift. In addition, according to the bathymetry
541 map of the region, the J fault is not connected to the Ghoubbet sea. The absence of the open cracks or
542 fractures observed with the November 1978 eruption in the southern zone of the Asal Rift is another
543 argument that limits the possibility of possible fluid flow or water infiltration in this sector, while the
544 presence of activated faults in 1978 in the northern part is dominant (Figure 1).
545 Wells A5, F1, and F2 were drilled in the north-east zone of the H fault, but only the temperature
546 profile of well A5 was available for this study (Figure 2). This temperature profile shows a first
547 convection cell from 300 to 500 m and a second convection cell from 500 to 1200 m, and then a constant
548 geothermal gradient that can be related to heat conduction between 1.2 and 1.8 km. This information,
549 therefore, correlates with the conductive zone to the north-east of fault H. Furthermore, the
550 geothermal gradient estimated between 1.2 and 1.8 km in well Asal 5 is 18.7 °C/100 m. In addition,
551 well Asal 5 is located in a relatively conductive zone with an electrical resistivity greater than
552 20 Ω m, which can corroborate the absence of groundwater that can have a high salinity associated
553 with electrical resistivity less than or equal to a value of 10 Ω m [21]. This Asal 5 well can be close to
554 a heat source where heat is transferred by deep conduction, resulting in a strong conductive
555 geothermal gradient at a depth between 1.2 and 1.8 km. The absence of groundwater circulation
556 between 1.2 and 2 km in this well is corroborated by both its temperature profile and the electrical
557 resistivity model presented in this study. The latter also shows the Fiɛale Caldera in close proximity
558 to well Asal 5 has a particular electrical resistivity range of 20–30 Ω m. It is highly probable that this
559 resistivity is characteristic of the nature of the rock in this Caldera zone, which can be hot, but less
560 permeable, limiting the circulation of fluid. Another important fact is that hydrothermal mineral
561 assemblage is in good agreement with the measured temperatures in all geothermal wells of Asal
562 Rift, except for well Asal 5 [39], where a chlorite-epidote mineral assemblage zone that normally
563 should exist at a high temperature was observed at a depth between 500 and 1200 m, where an

important temperature inversion was measured (Figure 2). This information is helpful allows to assume that a pre-existing high temperature reservoir can have existed before the infiltration of cold sea water, and the temperature inversion may likely be related to a recent infiltration of seawater.

Geodetic measurements indicate that the opening of the Asal–Ghoubbet Rift has a velocity of 16 mm/year and an opening direction perpendicular to the rift axis, highlighting the asymmetrical behavior of the Asal Rift [6]. These authors studied the horizontal and vertical deformation of the rift in directions parallel and perpendicular to the rift axis. They consider that the north-eastern part of the Asal Rift is the site of significant continuous deformation, whereas for its south-western part, the deformation is weak and practically non-existent. These results corroborate the presence of active normal faults in the north-eastern part of the rift and the existing seismic activity [4]. The rate of deformation along the axis perpendicular to the rift axis increases towards the northeast of the rift [6]. This is a surprising correlation between the increase in this deformation rate and the increase in electrical conductivity highlighted by the model developed in this work pointing in the same direction (Figure 4).

The regional groundwater flow affected by sea water was believed to be the main source of recharge to Asal Lake [3], but our simulation results show the groundwater flow is directed toward both the Asal Lake and the Ghoubbet Sea, with a maximum point on the SE side diving flow in the two directions and a pronounced flow to Asal Lake. This can limit the pontifical depth of penetration of sea water intrusions near the surface. In this case, recharge of Asal Lake can occur through aquifer (C1), potentially containing fossil seawater that is likely fed by a deep hydrothermal circulation. In all the different simulation scenarios, it is important to highlight the evidence of groundwater flow into Asal Lake and hydrothermal circulation beneath Asal Lake and the Ghoubbet sea.

The superposition of three permeable zones with the predominance of flow towards Asal Lake and the Ghoubbet sea are important elements to advance the hypothesis of the existence of a large hydrothermal system under the rift that would be compartmentalized into these three permeable zones, which can be individualized under the tectonic activity and the injection of a deep heat source since the formation of the rift over the geological time. The subsurface flow at a depth between 300 and 700 m (Figure 7) can be influenced by the Ghoubbet sea and the local rift topography, while the intermediate flow at a depth between 1200 and 2000 m (Figure 7) is interpreted as the result of the development of a hydrothermal system, and the deep flow can be linked to a deep hydrothermal circulation feed by a heat source originating from a deep magmatic system (Figure 7). The presence of the cap rock layer limits possible communications between the second permeable layer, identified here as a potential deep reservoir, and the shallow aquifer C1 (Figure 5 and 7), and facilitates the development of a hydrothermal reservoir in the formation, where this cap rock layer covers and helps to contain thermal energy in the potential deep reservoir.

Similar simulation results obtained with scenario 5 (Figure 7) support the idea that regional flow variation is not strongly influenced by the permeability anisotropy in layer C1 of the conceptual model (Figure 5). In other words, the regional flow is mainly controlled by tectonics that affect deep structures and allow the deep heat source to be directed to shallower geological strata and formations. Simulations with an isotropic permeability of 10^{-15} m^2 inside the deep reservoir and equal to 10^{-17} m^2 inside the heat source were conducted for scenario 3 to indirectly evaluate the vertical dependence of permeability, which can decrease with depth. The development of hot convection cells within this unit was less pronounced than in scenarios 1 and 2 (Figure 6 and 7). Scenarios with permeability dependent temperature (scenarios 1, 2, and 5) seem to be more realistic than scenario 3 with isotropic permeability. However, the results from scenario 3 are not representative of conceptual hydrothermal models proposed in previous studies [41,42], where hydrothermal activity is concentrated in areas with elevated topography. Hydrothermal activity in permeability dependent temperature scenarios better correlates with the central zone of high topography (Figure 6 and 7). In scenarios 1, 2, and 5, the lateral extension of the hydrothermal reservoir with the isotherm 210 °C becomes important compared with the results of scenarios 3 and 4 (Figure 6 and 7). This pattern is in good agreement with a previous study conducted in a tectonically active rift-ridge zone in Iceland [43]. The authors of this study confirm that emplacement and geometry of the upflow zones are mainly controlled by

616 the location and the permeability values of fault zones. The geometry, location, and permeability
617 values of fault zones remain the same in all the different scenarios for this study, but we deduce from
618 our results that the permeability dependent temperature rock formulated in both heat source and
619 potential deep reservoir can play a major role to reproduce a representative dynamic heat transfer in
620 hydrothermal systems. Permeability dependent temperature formulated solely for the heat source
621 unit may not produce significant variation when the potential deep reservoir is set with a constant
622 permeability like the simulated conditions of scenario 4. In addition, the results are approximately
623 the same as the results of scenario 3, where isotropic permeability was set for both the heat source
624 and potential deep reservoir units. In such cases, we hypothesize that permeability dependent
625 temperature would be an appropriate formulation in a hydrothermal system as in the Asal Rift, when
626 it is adopted for both the heat source and potential deep reservoir or, uniquely, for the potential deep
627 reservoir like in scenario 2.
628 The comparison between the temperature profile measured in the Asal 6 well and the
629 temperature simulated appears more realistic with scenarios 1, 2, and 5 compared with other
630 scenarios (Figure 8). This indicates that the conditions used are representative of the rift and the
631 associated thermal anomaly can be related to the injection of a magma forming a heat source and the
632 development of vertical conduits qualified as active faults to convey this internal thermal energy. In
633 scenario 4 (Figure 8), the system at the end of the simulation began to cooled down, as the
634 temperature at 100,000 years is less than the temperature measured in well Asal 6. It can be reasonable
635 to interpret this as a consequence of an extinguished deep hydrothermal fluid circulation inside the
636 heat source layer, where permeability could be higher than that assigned in scenario 4. However, the
637 shape of the simulated temperature profile at the location of well Asal 6 is maintained and has the
638 same appearance as the measured temperature in well Asal 6. Furthermore, the same reservoir was
639 recognized at a depth between 1050 and 1300 m in three wells, Asal 1, 3, and 6, and the geologic
640 formation hosting this reservoir is called Dalha basal, which has an average age of 4 to 9 My, where
641 temperatures measured in this reservoir range from 260 to 280 °C [33] and are close to the simulated
642 temperatures in this study. In addition, permeability anisotropy considered in scenario 5 inside the
643 C1 layer does not lead to cooling of the system and the simulated thermal state at well Asal 6 is close
644 to the measured one (Figure 8). It can be assumed that the thermal anomaly caused by this near-
645 surface groundwater flow has less effect at the global scale of the system. Nevertheless, the
646 assumption of pronounced horizontal flow near Asal Lake in scenario 5 is corroborated by our
647 interpreted conceptual model based on electrical resistivity inversion (Figure 5), where the thickness
648 of the shallow aquifer called C1 increases toward Asal Lake. As results of MT inversion and
649 numerical simulations showed, this study is focused for the potential deep reservoir between 1 and
650 3 km. The developed 2D model simulate a regional groundwater flow that gives a capture of fluid
651 circulation in a regional scale. Then, the lack of a better correlation between measured and simulated
652 temperature at Asal 6 well for the shallow part of the system above 600 m of depth (Figure 8) may be
653 related to a localized fractures or convections cells. Another possible interpretation would be resulted
654 by the difference of density fluid between the upper part of the system and the lower part. May be if
655 a higher density fluid (as saline fluid) was considered in the shallow part than the deeper part, the
656 shallow part of temperature profile measured at Asal 6 well could be well represented.
657 Temperatures measured in the thermal springs emerging on the periphery of Asal Lake range
658 from 30 to 90 °C [3], and the results of the different scenarios show approximate emergence
659 temperatures that corroborate with those measured in the thermal springs (Figure 7). Based on the
660 chemical and isotopic characteristic of water in the Asal region, three main types of water may co-
661 exist in the subsurface: seawater intrusion from Ghoubbet sea, Asal Lake water, and meteoric
662 infiltration probably originating from the meteoric water that transits from Asal Rift to Sakalol-
663 Harralol depression or/and the meteoric water coming from the deep circulating regional aquifer
664 [14]. The low temperature emergence observed in the hot springs of group Manda [3], their chemical
665 composition of which is close to that of seawater, and the high rate of flow show that seawater
666 circulation through the faults and fractures is the main source of their recharge [15]. This information
667 can be related to the emplacement of the hot springs group Manda that are close to the H fault and

668 are aligned more or less to this H fault and with two other major faults located south of the H fault
669 (Figure 1). Moreover, in this case, the information corroborates our hypothesis that seawater intrusion
670 occurs where faults/fractures exist (Figure 1 and 4).
671 Dissolved salts in water can change the phase conditions of liquid–vapor system and the phase
672 relation of saline water approximated by the H_2O-NaCl system is not the same as those of pure water
673 considered in this study. In conditions of an H_2O-NaCl system such as that of the Asal Rift, the
674 temperature and pressure of liquid–vapor co-existence are above the critical values of pure water
675 [44]. Despite that the fluid simulated from HYDROTHERM code is pure water [19], for saline
676 geothermal fluid, the emplacement depth of intrusion controls significantly whether phase
677 separation is dominantly carried out by boiling or by condensation [35]. Obviously, in this case,
678 numerical simulations considering a saline geothermal fluid are expected to reveal the presence of a
679 vapor phase, as proposed by the BRGM conceptual model [17]. This model is in good agreement with
680 the gas chemical results of the Asal fumaroles and the water stable isotope data of their steam
681 condensates [11], as well as the decrease of boron concentrations in the well geothermal fluids
682 evidenced by geochemical analyses [3].
683 The total flow rate of geothermal fluid produced in well Asal 3 showed a considerable decrease
684 of production rate and a decrease of bottom hole pressure, which were related to sulphide and silica
685 deposits in the well with a total dissolved solids (TDS) of 116,000 ppm [33], suggesting a high
686 potential of permeability reduction.
687 The δD and $\delta^{18}O$ water stable isotope data for the geothermal fluids of the Asal wells and for
688 some hot springs (Korilii, Eadkorar, and Eounda Alifitta groups; Figure 1) indicated contributions of
689 meteoric water [3]. This meteoric contribution probably originates from the meteoric water that
690 transits from Asal Rift to Sakalol-Harralol depression or/and the meteoric water coming from the
691 deep circulating regional aquifer [14]. These authors showed, in the area of Sakalol-Harralol, the
692 presence of hot springs, with high TDS Na-Cl waters, aligned in NW-SE along the main faults like in
693 the Asal Rift. The high altitude zones of rift margins at the north and south do not seem to be potential
694 recharge sources. However, a more representative numerical model can incorporate these zones and
695 be tested to confirm or invalidate these hypotheses. As suggested by [14], the existence of a deep
696 regional aquifer that may have a wide extension in Djibouti and where the Asal geothermal water
697 has apparently common features in terms of chemical and water isotope compositions is a good
698 argument to highlight the need for a numerical multiphase model developed at a large regional scale.
699 Coastal aquifers in Djibouti hosted geothermal water that could be more evolved in terms of water–
700 rock interaction between deep fossil water and sea water intrusions [38].

701 **5. Conclusions**

702 This study emphasizes the importance of fault activity and its role in hydrothermal circulation.
703 More specifically, the hypothesis of groundwater infiltration into Asal Lake is supported by
704 numerical flow and heat transfer simulations performed after considering an electrical resistivity
705 model of the area. The electrical conductivity model obtained after inversion of MT data indicates
706 that faults can act as conduits for the circulation of water, notably the H fault, where the hanging wall
707 of the fault behaves as a hydrogeological barrier. The variation of the electrical conductivity gradient
708 and its increase from the south-west to the north-east of the rift are in agreement with previous work
709 that brings to light the presence of horizontal and vertical deformation in the south-west to north-
710 east direction. The 2D numerical model of flow and heat transfer developed in this study was used
711 to better understand the groundwater flow and hydrothermal circulation. Furthermore, this model
712 confirmed that flow is generally controlled by the presence of faults acting as conduits and driven by
713 deep heat sources. Three flow zones were defined based on the interpretation of electrical resistivity
714 and temperature profiles. The temperature simulated with our model having these three zones is
715 correlated with the temperature measured in well Asal 6, and is thus considered representative of the
716 heat transfer dynamics of the system. These three flow zones are shallow groundwater flow affected
717 by seawater and topography, an intermediate flow with a hydrothermal circulation, and a deep flow
718 related to the hot hydrothermal circulation originating from the magmatic heat source.

719 In the context of geothermal energy research, future exploration drilling can be located either
720 along this major H fault or in the northeastern part of the rift to capture a significant flow of
721 geothermal fluid that mainly comes from the underground circulation heated by the strong
722 geothermal gradient existing under the Asal Rift. The target drilling zone could be the deep potential
723 reservoir unit down to a depth of 3 km to better intercept permeable zones containing supercritical
724 water or inside the potential deep reservoir at an intermediate depth between 1 and 2 km. The Fiɛale
725 Caldera and its surrounding zones should be avoided as the presence of hot rocks is thought to
726 produce low permeability in this area.
727 It could be interesting to complete the present study with a second electrical resistivity model
728 including more MT sites covering the entire surface area of the Asal–Ghoubbet Rift and extending to
729 the north-east of the rift, notably the north Ghoubbet zone, in order to better understand the limits of
730 the hydrothermal system identified in our study and to establish a correlation on a larger scale
731 between the electrical resistivity gradient and the deformation velocity gradient estimated by
732 geodetic measurements [6]. In other words, such a complementary study will help estimate which
733 are the underground circulation paths and proportions of seawater and meteoric water recharged
734 through the faults in the hydrothermal systems identified in this study. According to the water stable
735 isotopes data [14], infiltration of meteoric water can possibly occur from the meteoric water that
736 transits from Asal Rift to Sakalol-Harralol depression or/and the meteoric water coming from the
737 deep circulating regional aquifer. Similarly, the development of a 2D numerical model of flow and
738 heat transfer down to a depth of 10 km can help to elucidate the role of magmatic intrusion in the
739 deep hydrothermal circulation.
740

741 **Author Contributions:** Conceptualization, A.H.A., J.R., and B.G.; methodology, A.H.A.; validation, J.R., B.G.,
742 B.S., and A.H.A.; formal analysis, A.H.A.; investigation, A.H.A.; resources, J.R. and B.G.; data curation, A.H.A;
743 writing—original draft preparation, A.H.A., J.R., and B.G.; writing—review and editing, A.H.A., J.R., B.G., and
744 B.S.; visualization, A.H.A.; supervision, J.R. and B.G.; project administration, J.R.; funding acquisition, J.R. and
745 B.G. All authors have read and agreed to the published version of the manuscript.

746 **Funding:** This research was funded by the Islamic Development Bank through a PhD scholarship awarded to
747 the first author as well as research funds attributed by the Natural Sciences and Engineering Research Council
748 of Canada given to the second and third authors.

749 **Acknowledgments:** We would like to thank the contribution and support of the INRS. Gaeten Sakindi
750 (Electricity Company of Rwanda), Abdourahman Haga, Awaleh Abdi, and Djama Robleh (Ministry of Energy
751 and Natural Resources of the Republic Djibouti) are further acknowledged for their precious help on this project.

752 **Conflicts of Interest:** The authors declare no conflict of interest. The funders had no role in the design of the
753 study; in the collection, analyses, or interpretation of data; in the writing of the manuscript; or in the decision to
754 publish the results.

755 **Appendix A**

756 **Table A1.** Verification of mesh independence for simulation of scenario 1.

757

Number of elements	Temperature at 1600 m depth in Asal 6 well *T* (°C)	Absolute value of relative difference (%)
1200	238.931	---
2400	248.257	0.039
4000	254.387	0.024
4800	256.327	0.007
10,000	255.095	0.004

758

References

1. Bellani, S.; Gherardi, F. Thermal Overview of an Area NW of the Larderello Geothermal Field, Italy. GRC Trans. 2013, 37, 231–236.
2. Mlynarski, M.; Zlotnicki, J. Fluid circulation in the active emerged Asal rift (east Africa, Djibouti) inferred from self-potential and Telluric–Telluric prospecting. Tectonophysics 2001, 339, 455–472, doi:10.1016/s0040-1951(01)00127-5.
3. Sanjuan, B.; Michard, G.; Michard, A. Origine des substances dissoutes dans les eaux des sources thermales et des forages de la région Asal-Ghoubbet (République de Djibouti). J. Volcanol. Geotherm. Res. 1990, 43, 333–352, doi:10.1016/0377-0273(90)90060-s.
4. Doubre, C.; Manighetti, I.; Dorbath, L.; Dorbath, C.; Bertil, D.; Delmond, J.C. Crustal structure and magmato-tectonic processes in an active rift (Asal-Ghoubbet, Afar, East Africa): 2. Insights from the 23-year recording of seismicity since the last rifting event. J. Geophys. Res. Space Phys. 2007, 112, doi:10.1029/2006jb004333.
5. Doubre, C.; Peltzer, G. Fluid-controlled faulting process in the Asal Rift, Djibouti, from 8 yr of radar interferometry observations. Geology 2007, 35, 69, doi:10.1130/g23022a.1.
6. Vigny, C.; De Chabalier, J.-B.; Ruegg, J.-C.; Huchon, P.; Feigl, K.L.; Cattin, R.; Asfaw, L.; Kanbari, K. Twenty-five years of geodetic measurements along the Tadjoura-Asal rift system, Djibouti, East Africa. J. Geophys. Res. Space Phys. 2007, 112, doi:10.1029/2004jb003230.
7. Manighetti, I.; Tapponnier, P.; Gillot, P.Y.; Jacques, E.; Courtillot, V.; Armijo, R.; Ruegg, J.C.; King, G. Propagation of rifting along the Arabia-Somalia Plate Boundary: Into Afar. J. Geophys. Res. Space Phys. 1998, 103, 4947–4974, doi:10.1029/97jb02758.
8. Pinzuti, P.; Mignan, A.; King, G.C. Surface morphology of active normal faults in hard rock: Implications for the mechanics of the Asal Rift, Djibouti. Earth Planet. Sci. Lett. 2010, 299, 169–179, doi:10.1016/j.epsl.2010.08.032.
9. Stein, R.S.; Briole, P.; Ruegg, J.-C.; Tapponnier, P.; Gasse, F. Contemporary, Holocene, and Quaternary deformation of the Asal Rift, Djibouti: Implications for the mechanics of slow spreading ridges. J. Geophys. Res. Space Phys. 1991, 96, 21789–21806, doi:10.1029/91jb02118.
10. Correira, H.; Demange, J.; Fabriol, R.; Gerard, A.; Varet, J. Champ Géothermique d'Asal: Synthèse des Données Disponibles au 1er Janvier 1983; Final BRGM report 83 SGN 022 GTH, Orleans, France 1983.
11. Marini, L. Geochemistry of North Ghoubbat-Asal Region; Geothermica Italiana report 551-9-LUI, 1987.
12. Gadalia, A.; Traineau, H. Deux Champs Géothermiques de Rifts Océaniques Émergés: Krafla (Islande) et Asal (République de Djibouti. Une Étude Comparative des Contextes Géologiques et des Méthodes d'exploration; Final BRGM report 84 SGN 216 IRG, 1984.
13. D'Amore, F.; Giusti, D.; Abdallah, A. Geochemistry of the high-salinity geothermal field of Asal, Republic of Djibouti, Africa. Geothermics 1998, 27, 197–210, doi:10.1016/s0375-6505(97)10009-8.
14. Awaleh, M.O.; Boschetti, T.; Soubaneh, Y.D.; Baudron, P.; Kawalieh, A.D.; Dabar, O.A.; Ahmed, M.M.; Ahmed, S.I.; Daoud, M.A.; Egueh, N.M.; et al. Geochemical study of the Sakalol-Harralol geothermal field (Republic of Djibouti): Evidences of a low enthalpy aquifer between Manda-Inakir and Asal rift settings. J. Volcanol. Geotherm. Res. 2017, 331, 26–52, doi:10.1016/j.jvolgeores.2016.11.008.
15. Fouillac, C.; Fabriol, R.; Lundt, F. Champ Géothermique d'Asal. Synthèse des Données Hydrogéologiques et Géochimiques Disponibles au 1er Janvier 1983; Final BRGM report 83 SGN 022 GTH, 1983.
16. Houssein, D.E.; Axelsson, G. Geothermal resources in the Asal Region, Republic of Djibouti: An update with emphasis on reservoir engineering studies. Geothermics 2010, 39, 220–227, doi:10.1016/j.geothermics.2010.06.006.
17. Demange, J.; Puvilland, P. Champ Géothermique d'Asal. Synthèse des Données; Rapport C.F.G, 1993.
18. Hayba, D.O.; Ingebritsen, S.E. Multiphase groundwater flow near cooling plutons. J. Geophys. Res. Space Phys. 1997, 102, 12235–12252, doi:10.1029/97jb00552.
19. Kipp, K.L.; Hsieh, P.A.; Charlton, S.R. Guide to the Revised Ground-Water Flow and Heat Transport Simulator: HYDROTHERM—Version 3; USGS: Reston, VA, USA, 2008.
20. Yamaya, Y.; Alanis, P.K.B.; Takeuchi, A.; Cordon, J.M.; Mogi, T.; Hashimoto, T.; Sasai, Y.; Nagao, T. A large hydrothermal reservoir beneath Taal Volcano (Philippines) revealed by

812 magnetotelluric resistivity survey: 2D resistivity modeling. Bull. Volcanol. 2013, 75, 729,
813 doi:10.1007/s00445-013-0729-y.
814 21. Simpson, F.; Bahr, K. Practical Magnetotellurics, 1st ed.; Cambridge University Press:
815 Cambridge, UK, 2005.
816 22. Sakindi, G. Three-Dimensional Inversion of Magnetotelluric Data: Geological-Geothermal
817 Interpretation of Asal Geothermal Field, Djibouti. Master's Thesis, United Nations University,
818 Reykjavik, Iceland, 2015.
819 23. Szarka, L.; Menvielle, M. Analysis of rotational invariants of the magnetotelluric impedance
820 tensor. Geophys. J. Int. 1997, 129, 133–142, doi:10.1111/j.1365-246x.1997.tb00942.x.
821 24. Constable, S.C.; Parker, R.L.; Constable, C.G. Occam's inversion: A practical algorithm for
822 generating smooth models from electromagnetic sounding data. Geophysics 1987, 52, 289–300,
823 doi:10.1190/1.1442303.
824 25. Rung-Arunwan, T.; Siripunvaraporn, W.; Utada, H. On the Berdichevsky average. Phys. Earth
825 Planet. Inter. 2016, 253, 1–4, doi:10.1016/j.pepi.2016.01.006.
826 26. Rung-Arunwan, T.; Siripunvaraporn, W.; Utada, H. Use of ssq rotational invariant of
827 magnetotelluric impedances for estimating informative properties for galvanic distortion. Earth
828 Planets Space 2017, 69, 80, doi:10.1186/s40623-017-0665-8.
829 27. Spichak, V.; Manzella, A. Electromagnetic sounding of geothermal zones. J. Appl. Geophys.
830 2009, 68, 459–478, doi:10.1016/j.jappgeo.2008.05.007.
831 28. Sanford, W.E. A simulation of the hydrothermal response to the Chesapeake Bay bolide impact.
832 Geofluids 2005, 5, 185–201, doi:10.1111/j.1468-8123.2005.00110.x.
833 29. Driesner, T.; Geiger, S. Numerical Simulation of Multiphase Fluid Flow in Hydrothermal
834 Systems. Rev. Miner. Geochem. 2007, 65, 187–212, doi:10.2138/rmg.2007.65.6.
835 30. Raguenel, M.; Driesner, T.; Bonneau, F. Numerical modeling of the geothermal hydrology of the
836 Volcanic Island of Basse-Terre, Guadeloupe. Geotherm. Energy 2019, 7, 1–16, doi:10.1186/s40517-
837 019-0144-5.
838 31. Weis, P. The dynamic interplay between saline fluid flow and rock permeability in magmatic-
839 hydrothermal systems. Geofluids 2015, 15, 350–371, doi:10.1111/gfl.12100.
840 32. Gaudin, D.; Finizola, A.; Delcher, E.; Beauducel, F.; Allemand, P.; Delacourt, C.; Brothelande, E.;
841 Peltier, A.; Di Gangi, F. Influence of rainfalls on heat and steam fluxes of fumarolic zones: Six
842 months records along the Ty fault (Soufrière of Guadeloupe, Lesser Antilles). J. Volcanol.
843 Geotherm. Res. 2015, 302, 273–285, doi:10.1016/j.jvolgeores.2015.06.015.
844 33. Jalludin, M. State of Knowledge of Geothermal Provinces of Republic of Djibouti; UNU training
845 KENGEN: Naivasha, Kenya, 2007.
846 34. Vosteen, H.-D.; Schellschmidt, R. Influence of temperature on thermal conductivity, thermal
847 capacity and thermal diffusivity for different types of rock. Phys. Chem. Earth Parts A/B/C 2003,
848 28, 499–509, doi:10.1016/s1474-7065(03)00069-x.
849 35. Scott, S.; Driesner, T.; Weis, P. Boiling and condensation of saline geothermal fluids above
850 magmatic intrusions. Geophys. Res. Lett. 2017, 44, 1696–1705, doi:10.1002/2016gl071891.
851 36. Houssein, I.; Sanjuan, B.; Michard, G. Indices Géochimiques de l'Existence d'un Fluide à 210 °C
852 dans la Région d'Obock (République de Djibouti); Note au C.R.A.S, t.316, série II,, pp. 771–776,
853 1993.
854 37. Sanjuan, B. Use of a new Sodium/Lithium (Na/Li) geothermometric relationship for High-
855 Temperature (HT) geothermal fluids derived from seawater/basalt interaction processes:
856 Application to the Djibouti case. In Proceedings of the Third East African Rift Geothermal
857 Conference, Djibouti, 22–25 November 2010; p. 22.
858 38. Boschetti, T.; Awaleh, M.O.; Barbieri, M. Waters from the Djiboutian Afar: A Review of
859 Strontium Isotopic Composition and a Comparison with Ethiopian Waters and Red Sea Brines.
860 Water 2018, 10, 1700, doi:10.3390/w10111700.
861 39. Zan, L.; Gianelli, G.; Passerini, P.; Troisi, C.; Haga, A.O. Geothermal exploration in the republic
862 of djibouti: Thermal and geological data of the hanlé and asal areas. Geothermics 1990, 19, 561–
863 582, doi:10.1016/0375-6505(90)90005-v.

40. Smittarello, D.; Grandin, R.; De Chabalier, J.; Doubre, C.; Deprez, A.; Masson, F.; Socquet, A.; Saad, I. Transient deformation in the Asal-Ghoubbet Rift (Djibouti) since the 1978 diking event: Is deformation controlled by magma supply rates? J. Geophys. Res. Solid Earth 2016, 121, 6030–6052, doi:10.1002/2016jb013069.
41. Harris, R.N.; Fisher, A.T.; Chapman, D.S. Fluid flow through seamounts and implications for global mass fluxes. Geology 2004, 32, 725, doi:10.1130/g20387.1.
42. Schardt, C.; Anderson, T.F.; Raiswell, R. Controls on Heat Flow, Fluid Migration, and Massive Sulfide Formation of an Off-axis Hydrothermal System-- the Lau Basin Perspective. Am. J. Sci. 2006, 306, 103–134, doi:10.2475/ajs.306.2.103.
43. Lupi, M.; Geiger-Boschung, S.; Graham, C.M. Hydrothermal fluid flow within a tectonically active rift-ridge transform junction: Tjörnes Fracture Zone, Iceland. J. Geophys. Res. Space Phys. 2010, 115, doi:10.1029/2009jb006640.
44. Bischoff, J.L.; Pitzer, K.S. Liquid-vapor relations for the system NaCl-H2O: Summary of the P-T-x surface from 300° to 500 °C. Am. J. Sci. 1989, 289, 217248.